Hindawi
Journal of Sensors
Volume 2019, Article ID 2413408, 8 pages
https://doi.org/10.1155/2019/2413408

Research Article

A Feedback Method to Improve the Dynamic Range and the Linearity of Magnetoimpedance Magnetic Sensor

Dongfeng He

National Institute for Materials Science, Tsukuba, Ibaraki 305-0047, Japan

Correspondence should be addressed to Dongfeng He; he.dongfeng@nims.go.jp

Received 20 August 2019; Accepted 11 November 2019; Published 12 December 2019

Academic Editor: Stelios M. Potirakis

We developed a high-sensitivity magnetoimpedance magnetic field sensor using a FeCoSiB amorphous wire and a coil wound around it. The amorphous wire had the diameter of 0.1 mm and the length of 5 mm. The magnetic field resolution of about 20 pT/$\sqrt{}$Hz was achieved. But the dynamic range of the magnetoimpedance magnetic field sensor was only about ±0.7 Gauss, which was not enough for some applications, such as the defect evaluation of steel plate. The linearity of the system was also not good when big magnetic field was applied, which will cause some noise when the system is used in unshielded environment. We developed a feedback method to improve the dynamic range and the linearity of the magnetic field sensor. The operation point of the magnetic field sensor was fixed by sending a feedback current to the coil. Using the feedback method, the dynamic range was improved from ±0.7 Gauss to ±10 Gauss and the linearity was also improved over 100 times better. An eddy current testing system using the magnetic sensor was developed, and the crack defects in steel plate and in 3D-printed titanium alloy plate were evaluated.

1. Introduction

Room temperature-sensitive magnetic sensors have been developed and used in various areas of communication, geological exploration, medical diagnostics, nondestructive evaluation (NDE), and security control [1–10]. These sensors are normally operated in unshielded environment with big background interferences, such as the power line interference. To measure the small signal in the big background interferences, good linearity of the sensing system is important. Otherwise, the big background interferences may cause the distortion of the signal and increase the noise of the system.

For the NDE application of magnetic sensor, some ferromagnetic material samples may produce strong magnetic fields and cause the saturation of the magnetic sensors. Feedback methods are often used to increase the dynamic ranges of magnetic sensors and improve the linearity of magnetic sensors [11–13].

Using the $(Fe_{0.06}Co_{0.94})_{72.5}Si_{12.5}B_{15}$ (FeCoSiB) amorphous wire with the diameter of 0.1 mm and the length of 5 mm, we developed a high-sensitivity magnetoimpedance (MI) sensor [14]. There was no electrical connection with the amorphous wire. The DC bias current and the AC current flow in the coil directly. In this paper, we present our new results of the high-sensitivity MI sensor and a feedback method to improve the dynamic range and the linearity of the magnetic sensing system. We also constructed the eddy current testing (ECT) system with the magnetic sensor and used it to evaluate the crack defect of 3D-printed titanium alloy and steel plate.

2. MI Magnetic Sensor without Feedback

Figure 1 shows the schematic block diagram of the MI magnetic field sensor made using the FeCoSiB amorphous wire and the driving circuit without feedback. The sensor element was composed of a FeCoSiB amorphous wire and a coil wound around it. Different from normal MI sensor, there was no electrical connection with the amorphous wire. To make it capable of measuring the applied DC magnetic field, DC bias current and AC bias current were used in the driving circuit. The inductor L_D and the capacitors of C1 and C2 were used to isolate the DC bias current, the AC bias current, and the voltage signal across the coil. The magnetic sensor is

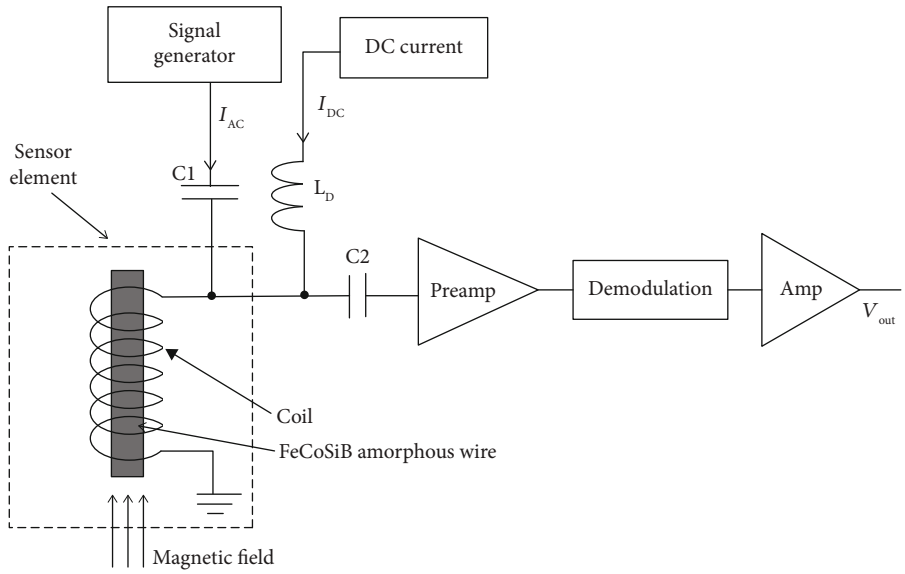

Figure 1: Schematic block diagram of the magnetic field sensor made using the FeCoSiB amorphous wire and the driving circuit without feedback.

used to measure the magnetic field along the direction of the amorphous wire.

In our experiments, the length of the FeCoSiB amorphous wire was 5 mm and the diameter was 0.1 mm. The coil wound around the amorphous wire was 30 turns wrapped using a copper wire with a diameter of 0.1 mm. The diameter of the coil was about 0.6 mm. The DC bias current was about 50 mA, and the amplitude of the AC bias current was about 20 mA. The frequency of the AC bias current ranged from 100 kHz to 5 MHz, and maximum signal amplitudes were achieved when the frequency was between 1 MHz and 2 MHz. In this paper, we used the frequency of 1 MHz.

Figure 2 shows the *B-H* curve of the FeCoSiB amorphous wire and the principle of the MI magnetic field sensor. The DC bias current I_{DC} in Figure 1 produced the DC magnetic field H_{DC}, and the AC bias current I_{AC} in Figure 1 produced the AC magnetic field H_{AC}, V_{AC} was the voltage across the coil wound around the amorphous wire. If H_{DC} was small, the sensor element operated in the linear part of the *B-H* curve, the amplitude of V_{AC} did not change with the external applied DC or low-frequency magnetic field. It could not be used to measure the DC magnetic field. If the DC bias current was increased and H_{DC} was near to the saturation corner of the *B-H* curve, the amplitude of V_{AC} changed with the external DC or low-frequency magnetic field.

Figure 3(a) shows the voltage signal when the external applied magnetic field was 0 Gauss. The signal amplitude was about 100 mV. Figure 3(b) shows the voltage signal when the external applied magnetic field was 1 Gauss. The signal amplitude was about 80 mV. The signal amplitude changed with the applied DC magnetic field.

In the driving circuit shown in Figure 1, the preamplifier with the gain of 30 dB was used to amplify the 1 MHz AC voltage signal. The demodulation was used to get the amplitude signal of the AC voltage signal, and the output voltage of V_{out} was used to measure the external DC or low-frequency magnetic field. We measured the output voltage changing with the applied external magnetic field. Figure 4 shows the results. For the applied external magnetic field between -0.7 Gauss and +0.7 Gauss, the magnetic field response of the magnetic sensor was nearly linear.

Figure 5 shows the magnetic field noise spectrum of the magnetic sensor with amorphous wire. The magnetic field noise spectrum was measured in a three-layer permalloy shielding box. The peaks on the spectrum were the 50 Hz inference and its harmonics. The magnetic field resolution of about 20 pT/$\sqrt{}$Hz was obtained.

To observe the distortion of the output signal of the magnetic field sensor, we applied a 30 Hz sine wave magnetic field to the sensor by putting the sensor in the centre of a Helmholtz coil, and the Helmholtz coil was connected with a 30 Hz sine wave current source. For the sensor without feedback, if the applied field was small and in the linear range of the magnetic field sensor, the distortion of the signal was small. Figure 6 shows the output signal when the amplitude of the 30 Hz applied magnetic field was 0.2 Gauss (0.02 mT). If the applied field was big and exceeded the linear range of the magnetic field sensor, the distortion of the signal was big. Figure 7 shows the output signal when the amplitude of the 30 Hz applied magnetic field was 2 Gauss (0.2 mT).

Figure 8 shows the spectrum of the output signal for the 30 Hz applied magnetic field with the amplitude of 2 Gauss. Due to the signal distortion, the amplitudes of the harmonics were quite big.

Total harmonic distortion (THD) is normally used to evaluate the nonlinearity of magnetic sensing systems [15–17]. When a sinusoidal magnetic field is applied to the magnetic sensor, the THD of the output signal can be defined

$$\mathrm{THD} = \frac{\sqrt{A_2^2 + A_3^2 + \cdots}}{A_1}, \quad (1)$$

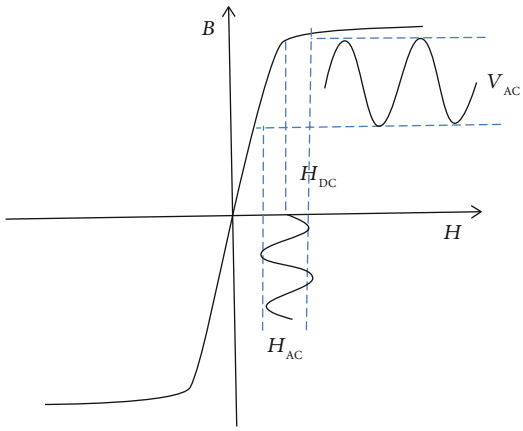

Figure 2: The *B-H* curve of the FeCoSiB amorphous wire and the principle of MI magnetic field sensor.

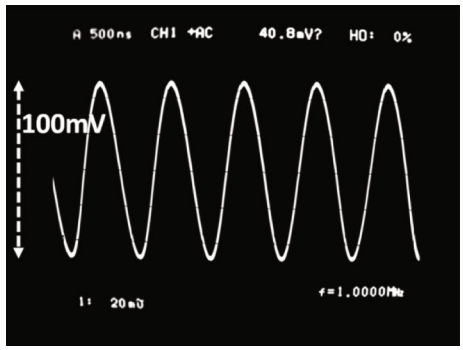

(a)

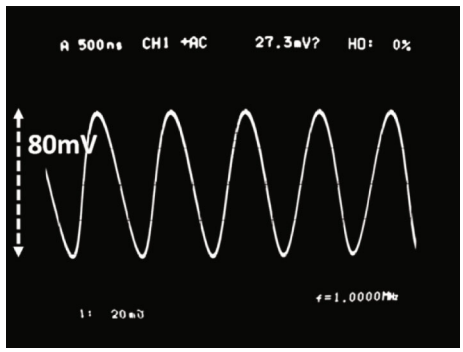

(b)

Figure 3: Voltage signal across the coil for different applied DC fields. (a) The signal when the applied field was zero. (b) The signal when the applied field was 1 Gauss.

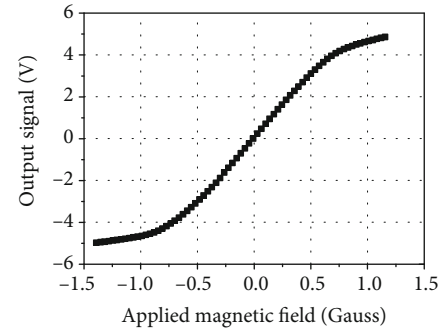

Figure 4: Output voltage of the magnetic sensor without feedback changes with the applied external magnetic field.

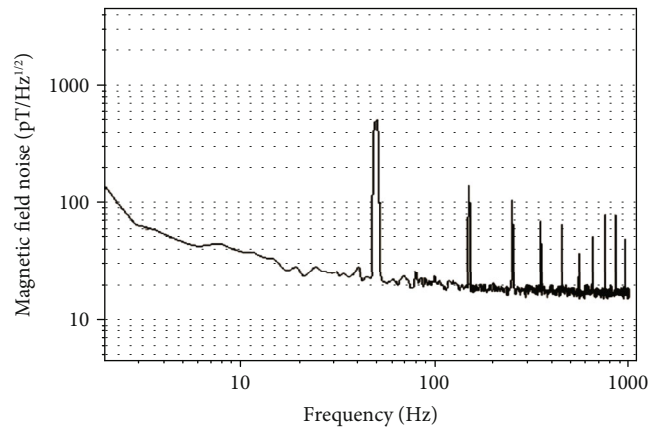

Figure 5: Magnetic field noise spectrum of the magnetic sensor measured in a permalloy shielding box.

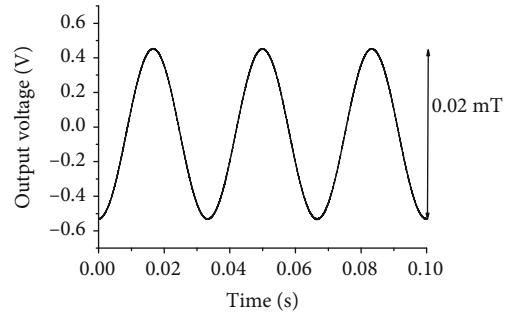

Figure 6: Output signal of the magnetic field sensor without feedback for the 30 Hz applied magnetic field with the amplitude of 0.2 Gauss (0.02 mT).

where A_1 is the signal amplitude of the fundamental frequency f; $A_2, A_3, \ldots$ are the amplitudes of the harmonics with the frequencies of $2f$, $3f$, …, which can be measured by a spectrum analyzer.

Figure 9 shows the experimental setup to measure the THD of the GMI sensor. The coil connected with the sine wave generator was used to produce the applied magnetic field. The harmonic distortion of the signal generated by the generator was below 5×10^{-4}. A spectrum analyzer was used to measure the THD of the output signals of the MI magnetic field sensor. To measure the small harmonic signals accurately, the influence of fundamental frequency signal must be reduced. A resistance trimmer was used to suppress the fundamental frequency signal of MI sensor output. By this method, the influence of the harmonics of the input signal could also be reduced.

In the measurement, the resistance of R1 was first adjusted to make the output of the MI magnetic field sensor be equal to the voltage of the sine wave generator; then, the resistance trimmer R2 was adjusted to cancel the fundamental signal of the sensor output. We estimated that the relative error of our measurement was about 10%.

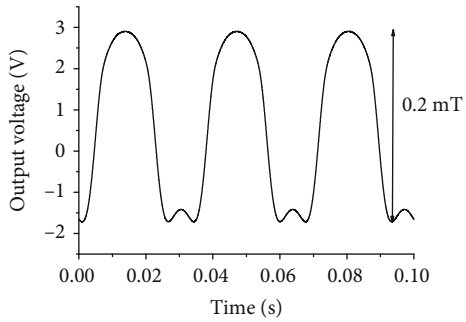

Figure 7: Output signal of the magnetic field sensor without feedback for the 30 Hz applied magnetic field with the amplitude of 2 Gauss (0.2 mT).

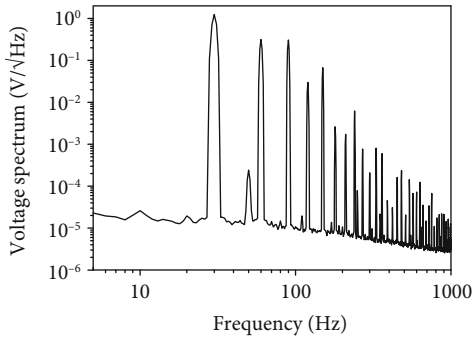

Figure 8: Output voltage spectrum of the MI magnetic field sensor without feedback for the 30 Hz applied magnetic field with the amplitude of 2 Gauss.

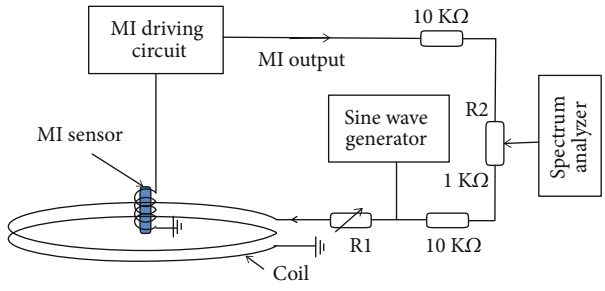

Figure 9: Setup of nonlinearity measurement.

Figure 10 shows the THD of the sensor without feedback for the 30 Hz applied magnetic field. It increased with the amplitude of the applied magnetic field.

3. MI Magnetic Sensor with Feedback

Magnetic feedback method is a good way to increase the linearity of magnetic sensor [18]. Figure 11 shows the block diagram of the MI magnetic field sensor with feedback. After the demodulation and an amplifier, an integrator was used. A feedback current produced by the output of the integrator and the feedback resistor R_F was sent to the coil wrapped around the amorphous wire. The magnetic field produced by the feedback current automatically compensated the

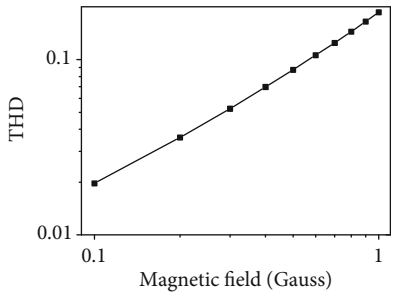

Figure 10: THD of MI magnetic field sensor without feedback for the 30 Hz applied magnetic field with different amplitudes.

applied magnetic field. Thus, the operation point of the MI magnetic field sensor was fixed. By this way, the dynamic range and the linearity of the system can be dramatically improved. When the switch SW was off, the driving circuit operated in amplifier mode. The output voltage V of the amplifier responded to the magnetic field. When the switch SW was on, the driving circuit operated in feedback mode. A feedback current V_{out}/R_F was produced, and the magnetic field produced by the feedback current was equal to the applied magnetic field. Thus, the output voltage V_{out} was proportional to the applied magnetic field.

Figure 12 shows the output voltage of the MI magnetic field sensor with feedback changing with the applied external magnetic field. We can see that the linearity was very good for the applied external magnetic field between -10 Gauss and +10 Gauss. Compared with Figure 4, the dynamic range and the linearity were much improved.

With the feedback, the magnetic field resolution of the MI magnetic field sensor was similar with that of without feedback. To check the magnetic field resolution, a small 30 Hz magnetic field with the amplitude of about 2 nT was applied. Figure 13 shows the output signal of the MI magnetic sensor. To remove the 50 Hz inference, the observation bandwidth was about 40 Hz.

Figure 14 shows the output signal of the MI magnetic field sensor with feedback when the amplitude of the 30 Hz applied magnetic field was 2 Gauss (0.2 mT); and Figure 15 shows the output signal when the amplitude was 20 Gauss (2 mT). The distortions of the signals were very small even for a strong magnetic field of 2 mT. The feedback method was effective to improve the linearity of the magnetic field sensor.

Figure 16 shows the spectrum of the output signal of the MI magnetic field sensor with feedback for the 30 Hz applied magnetic field with the amplitude of 2 Gauss. Compared with the spectrum of the output signal without feedback shown in Figure 8, the amplitudes of the 30 Hz harmonics were much small.

Using the setup shown in Figure 9, we also measured the THD of the MI magnetic sensor with feedback for the 30 Hz applied magnetic field with different amplitudes. Figure 17 shows the results. For the amplitude of 1 Gauss, the THD of the signal with feedback was about 1.4×10^{-4}, which was about 1% of the THD value without feedback. The linearity can be much improved using the feedback method.

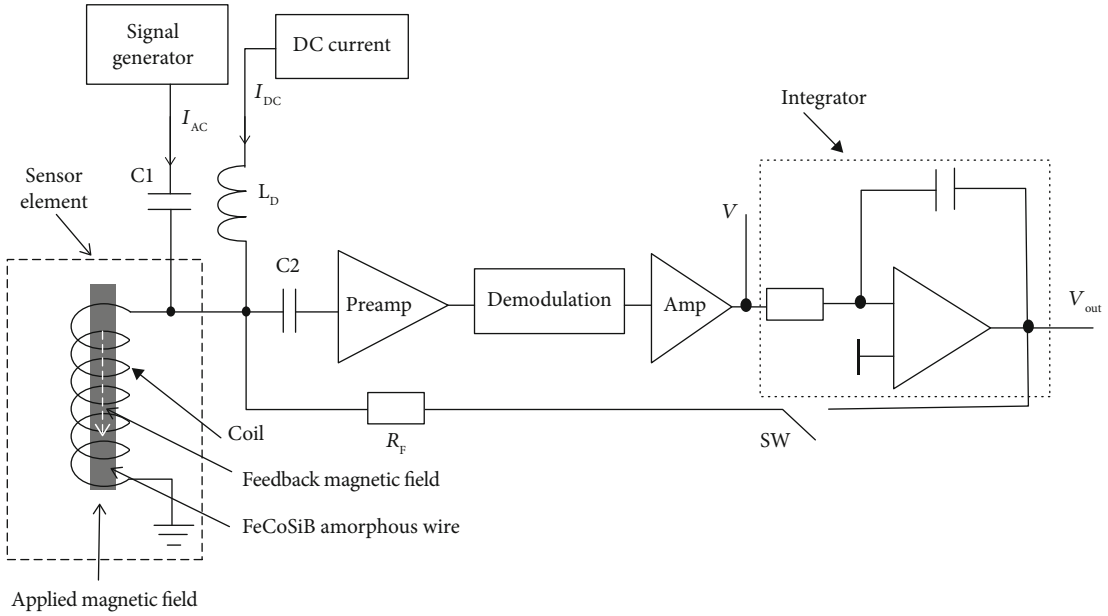

Figure 11: Block diagram of the MI magnetic field sensor and the driving circuit with feedback.

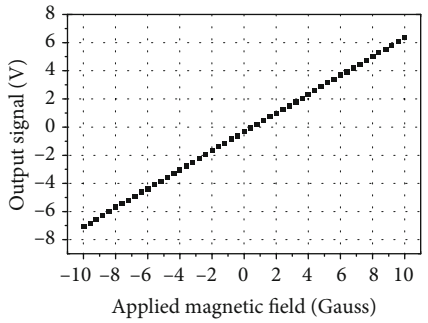

Figure 12: Output voltage of the magnetic sensor with feedback changes with the applied external magnetic field.

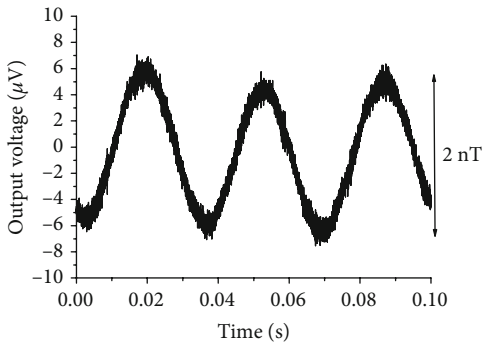

Figure 13: Output signal of the magnetic field sensor for the 30 Hz applied magnetic field with the amplitude of 2 nT.

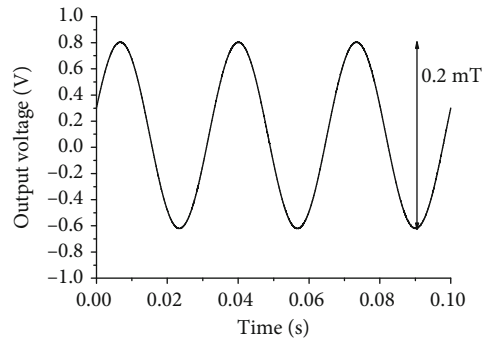

Figure 14: Output signal of the magnetic field sensor for the 30 Hz applied magnetic field with the amplitude of 2 Gauss (0.2 mT).

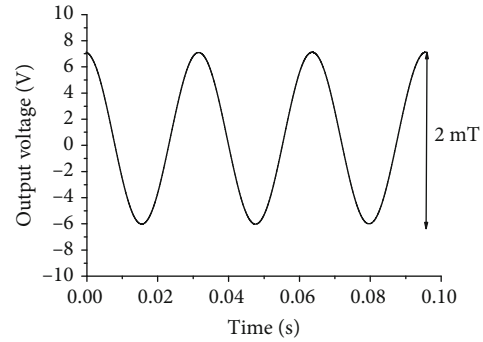

Figure 15: Output signal of the magnetic field sensor for the 30 Hz applied magnetic field with the amplitude of 20 Gauss (2 mT).

4. Eddy Current Testing Using MI Magnetic Sensor with Feedback

Figure 18 shows the block diagram of the ECT system using the MI magnetic field sensor with feedback. The excitation coil was 10 turns with the diameter of approximately 1 mm and was also wrapped around the FeCoSiB amorphous wire. The sine wave output of the lock-in amplifier was sent to the excitation coil to produce the excitation magnetic field. The excitation frequency was 20 kHz and the current amplitude was 20 mA. The amplitude of the magnetic field in the centre

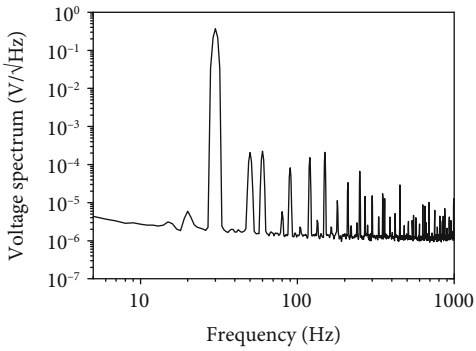

Figure 16: Output voltage spectrum of the MI magnetic field sensor with feedback for the 30 Hz applied magnetic field with the amplitude of 2 Gauss.

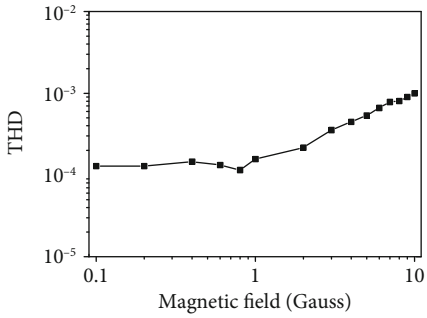

Figure 17: THD of MI magnetic field sensor with feedback for the 30 Hz applied magnetic field with different amplitudes.

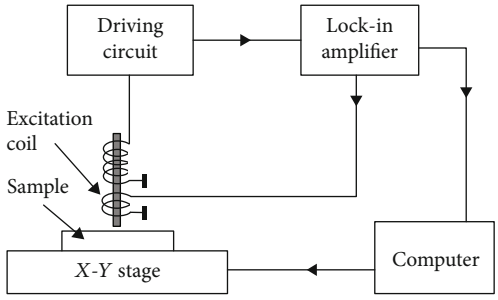

Figure 18: Block diagram of the ECT system with amorphous wire magnetic sensor.

of the excitation coil was about 2 Gauss. The MI magnetic field sensor was used to measure the magnetic field produced by the eddy current in the sample. The sample was put on an X-Y stage for the scanning. Figure 19 shows the photo of the setup.

Figure 20 shows the Ti-6L-4V titanium alloy sample fabricated by 3D laser printing. The size of the sample was 50 $\times$ 50 $\times$ 10 mm. There were two surface flaws extending from the edges of the sample. The length of flaw a was about 13 mm with the depth of about 1.5 mm, and the width of flaw a was from 0.2 mm to about 10 μm. The length of flaw b was about 15 mm with the depth of about 5 mm, and the width of flaw b was from 0.3 mm to about 10 μm.

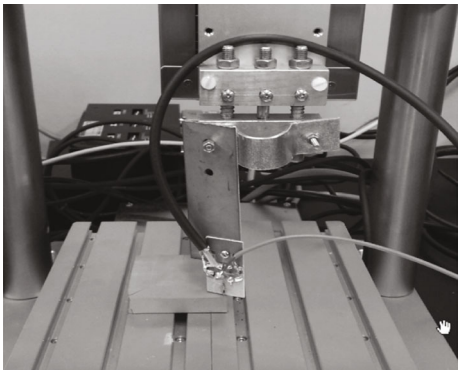

Figure 19: Photo of the ECT setup.

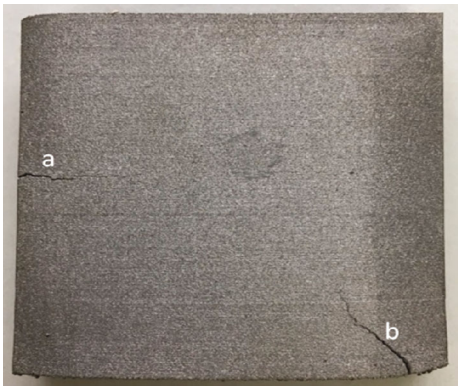

Figure 20: Photo of titanium alloy sample fabricated by a 3D laser printer.

Figure 21 shows the ECT result using the amorphous wire magnetic sensor. The scanning area was 45 mm $\times$ 45 mm and scanning step was 0.2 mm. The amplitude output signal of the lock-in amplifier was used to plot the 2D graph. The defects were displayed clearly.

We also evaluated the defect in the steel plate using the ECT system. The thickness of the steel plate was 3 mm. In the steel plate, there was a small hole defect with the size of about 1.5 mm and the depth of about 2 mm. The steel plate produced a strong magnetic field of about 5 Gauss. The MI magnetic sensor with feedback could operate well during scanning. An excitation coil with the diameter of about 3 mm was used.

The determination of the excitation frequency is an important factor in ECT, because the penetration of eddy current is limited by the skin effect. The skin depth is defined by $\delta = (\pi f \mu \sigma)^{-1/2}$, where δ is the skin depth, μ is the magnetic permeability, σ is the electrical conductivity, and f is the frequency. For the steel plate, the conductivity σ is about 2 $\times$ 106 S/m, the relative permeability is about 100, and the penetration depth is about 2.7 mm at the frequency of 170 Hz.

To detect deep defect in the steel plate, a lower excitation frequency of 170 Hz was used. The amplitude of the excitation current was about 20 mA. Figure 22 shows the

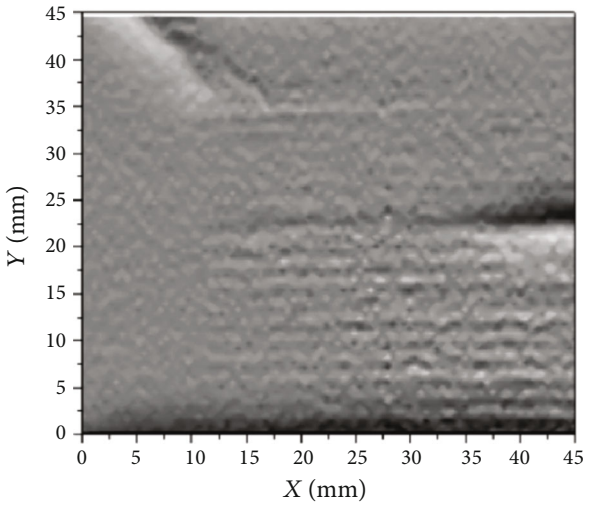

Figure 21: Scanning results by the ECT system with amorphous wire magnetic sensor.

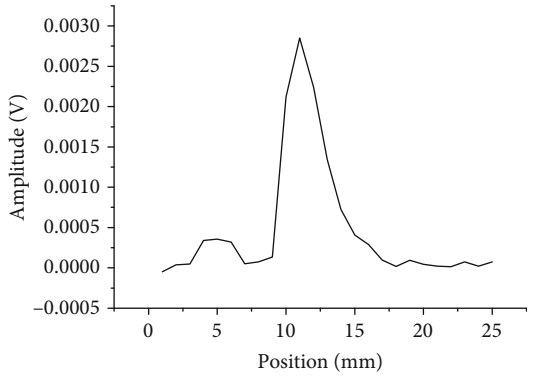

Figure 22: One scanning signal of a defect in the steel plate.

defect signal of one scanning, and Figure 23 shows the 2D scanning results.

5. Conclusion

A feedback method was developed for the MI magnetic field sensor. Using the feedback method, the dynamic range of the MI sensor was improved from ±0.7 Gauss to ±10 Gauss, and the linearity of the magnetic sensing system was also improved. The THD of the output signal with the feedback was about 1% of the THD without feedback.

If the MI sensor is used in an industrial environment, the amplitude of the 50 Hz line interference can be up to 1 μT. For the MI sensor without feedback, the signal distortion caused by the nonlinearity is about 10 nT, which is big enough to influence the accuracy of the detection. For the MI sensor with feedback, the signal distortion is about 100 pT, which is close to the magnetic field noise of the GMI sensor and has less influence to the accuracy of the detection. Therefore, for the applications in the industrial environment, the MI sensor with feedback is necessary.

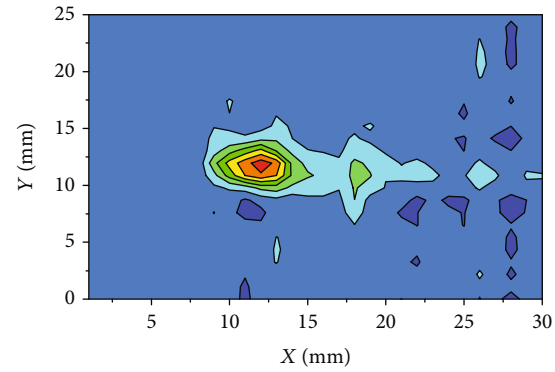

Figure 23: 2D scanning result of the defect in the steel plate.

We constructed the ECT system using the MI magnetic field sensor with feedback. Because of its big dynamic range, it can be used to evaluate defects in the steel plate. We will find more industrial applications for our magnetic field sensing system.

Data Availability

The ASCII data used to support the findings of this study were supplied by Dongfeng He under license and so cannot be made freely available. Requests for access to these data should be made to Dongfeng He (he.dongfeng@nims.go.jp).

Conflicts of Interest

The author declares that he has no conflicts of interest.

References

[1] L. V. Panina, K. Mohri, K. Bushida, and M. Noda, "Giant magneto-impedance and magneto-inductive effects in amorphous alloys (invited)," *Journal of Applied Physics*, vol. 76, no. 10, pp. 6198–6203, 1994.

[2] L. G. C. Melo, D. Ménard, A. Yelon, L. Ding, S. Saez, and C. Dolabdjian, "Optimization of the magnetic noise and sensitivity of giant magnetoimpedance sensors," *Journal of Applied Physics*, vol. 103, no. 3, article 033903, 2008.

[3] K. Mohri, F. B. Humphrey, L. V. Panina et al., "Advances of amorphous wire magnetics over 27 years," *Physica Status Solidi*, vol. 206, no. 4, pp. 601–607, 2009.

[4] S. Dwevedi, G. Sreenivasulu, and G. Markandeyulu, "Contact and non-contact magnetoimpedance in amorphous and nanocrystalline $Fe_{73.5}Si_{13.5}B_8CuV_3Al$ ribbons," *Journal of Magnetism and Magnetic Materials*, vol. 322, no. 3, pp. 311–314, 2010.

[5] K. Mohri, T. Uchiyama, L. P. Shen, C. M. Cai, and L. V. Panina, "Amorphous wire and CMOS IC-based sensitive micro-magnetic sensors (MI sensor and SI sensor) for intelligent measurements and controls," *Journal of Magnetism and Magnetic Materials*, vol. 249, no. 1-2, pp. 351–356, 2002.

[6] M. Tibu and H. Chiriac, "Amorphous wires-based magneto-inductive sensor for nondestructive control," *Journal of Magnetism and Magnetic Materials*, vol. 320, no. 20, pp. e939–e943, 2008.

[7] T. Uchiyama, S. Nakayama, K. Mohri, and K. Bushida, "Biomagnetic field detection using very high sensitivity magnetoimpedance sensors for medical applications," *Physica Status Solidi A: Applications and Materials Science*, vol. 206, no. 4, pp. 639–643, 2009.

[8] D. F. He, Z. Wang, M. Kusano, S. Kishimoto, and M. Watanabe, "Evaluation of 3D-Printed titanium alloy using eddy current testing with high-sensitivity magnetic sensor," *NDT & E International*, vol. 102, pp. 90–95, 2019.

[9] T. Uchiyama and J. J. Ma, "Design and demonstration of novel magnetoencephalogram detectors," *IEEE Transactions on Magnetics*, vol. 55, no. 7, pp. 1–8, 2019.

[10] K. N. Choi, "Metal detection sensor utilizing magneto-impedance magnetometer," *Journal of Sensors*, vol. 2018, Article ID 3675090, 9 pages, 2018.

[11] D. F. He, M. Daibo, and M. Yoshizawa, "Mobile HTS rf SQUID magnetometer," *IEEE Transactions on Applied Superconductivity*, vol. 13, no. 2, pp. 200–202, 2003.

[12] D. F. He, M. Tachiki, and H. Itozaki, "Highly sensitive anisotropic magnetoresistance magnetometer for Eddy-current nondestructive evaluation," *The Review of Scientific Instruments*, vol. 80, no. 3, article 036102, 2009.

[13] D. Drung, "High-T_c and low-T_c dc SQUID electronics," *Superconductor Science & Technology*, vol. 16, no. 12, pp. 1320–1336, 2003.

[14] D. F. He and M. Shiwa, "A magnetic sensor with amorphous wire," *Sensors*, vol. 14, no. 6, pp. 10644–10649, 2014.

[15] D. G. Nichols, E. Dantsker, R. Kleiner, M. Mück, and J. Clarke, "Linearity of high-T_c dc superconducting quantum interference device operated in a flux-locked loop," *Journal of Applied Physics*, vol. 80, no. 10, pp. 6032–6038, 1996.

[16] J. Beyer, D. Drung, F. Ludwig, and T. Schurig, "Linearity of sensitive $YBa_2Cu_3O7_{-x}$ dc superconducting quantum interference device magnetometers," *Journal of Applied Physics*, vol. 86, no. 6, pp. 3382–3386, 1999.

[17] D. F. He, Y. Zhang, A. I. Braginski, Y. D. Dai, and S. Z. Wang, "The nonlinearity of the high-Tc rf SQUID system," *Physica C: Superconductivity*, vol. 341-348, Part 4, pp. 2695-2696, 2000.

[18] D. F. He and M. Shiwa, "High sensitive magnetic sensor with amorphous wire," in *2015 9th International Conference on Sensing Technology (ICST)*, pp. 8–10, Auckland, New Zealand, December 2015.